

Early identification of subjective cognitive decline using 2D horizontal visibility graph analysis of structural MRI networks

Huang-Jing Ni(倪黄晶), Yu-Fei Dai(戴雨菲), Ye Wu(吴烨), Jiao-Long Qin(秦姣龙), and for the Alzheimer's Disease Neuroimaging Initiative (ADNI)

Citation: Chin. Phys. B, 2026, 35 (**8**): 088701. DOI: 10.1088/1674-1056/ae2670
http://cpb.iphy.ac.cn; http://iopscience.iop.org/cpb

What follows is a list of articles you may be interested in

Explosive information spreading in higher-order networks: Effect of social reinforcement

Yu Zhou(周宇), Yingpeng Liu(刘英鹏), Liang Yuan(袁亮), Youhao Zhuo(卓友濠), Kesheng Xu(徐克生), Jiao Wu(吴娇), and Muhua Zheng(郑木华)

Chin. Phys. B, 2025, 34 (**3**): 038704. DOI: 10.1088/1674-1056/adacc8

Effects of individual heterogeneity on social contagions

Fu-Zhong Nian(年福忠) and Yu Yang(杨宇)

Chin. Phys. B, 2024, 33 (**5**): 058705. DOI: 10.1088/1674-1056/ad225e

Dynamical behaviors in discrete memristor-coupled small-world neuronal networks

Jieyu Lu(鲁婕妤), Xiaohua Xie(谢小华), Yaping Lu(卢亚平), Yalian Wu(吴亚联), Chunlai Li(李春来), and Minglin Ma(马铭磷)

Chin. Phys. B, 2024, 33 (**4**): 048701. DOI: 10.1088/1674-1056/ad1483

Studying the co-evolution of information diffusion, vaccination behavior and disease transmission in multilayer networks with local and global effects

Liang'an Huo(霍良安) and Bingjie Wu(武兵杰)

Chin. Phys. B, 2024, 33 (**3**): 038702. DOI: 10.1088/1674-1056/ad0114

Impact of individual behavior adoption heterogeneity on epidemic transmission in multiplex networks

Liang'an Huo(霍良安) and Yue Yu(于跃)

Chin. Phys. B, 2023, 32 (**10**): 108703. DOI: 10.1088/1674-1056/acea65

Early identification of subjective cognitive decline using 2D horizontal visibility graph analysis of structural MRI networks

Huang-Jing Ni(倪黄晶)[1,†], Yu-Fei Dai(戴雨菲)[1], Ye Wu(吴烨)[2], Jiao-Long Qin(秦姣龙)[2,‡], and for the Alzheimer's Disease Neuroimaging Initiative (ADNI)

[1] *School of Computer Science, Nanjing University of Posts and Telecommunications, Nanjing* 210003, *China*

[2] *Key Laboratory of Intelligent Perception and Systems for High-Dimensional Information of Ministry of Education, School of Computer Science and Engineering, Nanjing University of Science and Technology, Nanjing* 210094, *China*

(Received 3 September 2025; revised manuscript received 23 November 2025; accepted manuscript online 2 December 2025)

Subjective cognitive decline (SCD) represents a preclinical stage of Alzheimer's disease, yet objective evaluation criteria for early diagnosis remain lacking. Traditional morphometric indicators, such as gray matter volume or density, overlook local voxel features and inter-voxel associations. To address this limitation, this study introduces a two-dimensional horizontal visibility graph (2DHVG) analysis method to identify brain structural abnormalities in SCD patients. Each axial slice of gray matter images was converted into a 2DHVG, and complex network features, including clustering coefficient and betweenness centrality, were extracted to characterize local connectivity and global information transmission capacity. Principal component analysis and light gradient boosting machine were employed for feature selection and classification. The 2DHVG-based method achieved excellent performance in SCD identification, with a mean classification AUC of 0.958, mean accuracy of 89.0%, mean sensitivity of 86.1%, mean specificity of 90.3%, and mean F1-score of 82.9%. Furthermore, significant positive correlations were observed between the mean clustering coefficient and both ADNI working memory (ADNI_MEM, $R = 0.3339$, $P = 0.0014$) and learning ability indicators (RAVLT.learning, $R = 0.3531$, $P = 0.0007$). The mean betweenness centrality similarly correlated with ADNI_MEM ($R = 0.3018$, $P = 0.0041$) and RAVLT.learning ($R = 0.3149$, $P = 0.0027$). The 2DHVG-based structural imaging analysis method demonstrates significant advantages in feature extraction and classification modeling, providing novel insights for graph-theoretic modeling of structural MRI data in early SCD identification.

Keywords: subjective cognitive decline, horizontal visibility graph, complex network, structural magnetic resonance imaging

PACS: 87.57.–s, 05.10.–a, 87.19.lf, 98.52.Cf

DOI: 10.1088/1674-1056/ae2670 **CSTR:** 32038.14.CPB.ae2670

1. Introduction

Subjective cognitive decline (SCD) is an important preclinical stage of Alzheimer's disease (AD).[1] It is characterized by individuals' self-reported perception of cognitive decline in the absence of objective cognitive impairment as evaluated by standard neuropsychological assessments. The early detection of SCD faces major challenges, largely due to the lack of highly specific and minimally invasive markers. In current clinical practice, the diagnosis of SCD partly relies on invasive biomarkers, such as cerebrospinal fluid analysis,[2] which are both costly and unsuitable for large-scale population screening. Recently, structural magnetic resonance imaging (sMRI) has emerged as an ideal platform for detecting early and subtle structural brain changes in patients with SCD,[3] and is expected to become a crucial tool for monitoring the preclinical pathological progression of AD.

Conventional sMRI-based studies of SCD have focused on morphological indicators such as gray matter volume or density.[4] Previous studies have shown that patients with SCD have significantly lower gray matter volumes than healthy controls in regions of the medial temporal lobe,[5,6] the amygdala,[7,8] the hippocampus,[9,10] and the internal olfactory cortex.[11,12] In addition, regions such as the frontal cortex[13] and insula[14] also showed structural abnormalities. However, these traditional analysis methods have inherent limitations: they quantify brain structural changes by accumulating pixel gray values or calculating regional averages, which can detect macroscopic structural atrophy but are difficult to reveal the topological dynamics of gray matter microstructures. These methods implicitly treat brain regions as functionally or structurally independent and pixels as isolated units, failing to quantify spatial correlations and patterns of information exchange between pixels. This challenge is particularly evident in the early identification of SCD, since the core pathology involves microscopic network damage rather than simple volume atrophy.[15] Traditional morphological metrics are insufficiently sensitive in capturing these early, subtle changes in network topology, and there is an urgent need to

[†]Corresponding author. E-mail: nihuangjing@njupt.edu.cn

[‡]Corresponding author. E-mail: jiaolongq@njust.edu.cn

© 2026 Chinese Physical Society and IOP Publishing Ltd. All rights, including for text and data mining, AI training, and similar technologies, are reserved.

develop finer methods for analyzing topological dynamics.

In recent years, complex network theory has begun to be applied to sMRI analysis, e.g., voxel-based 3D structural covariance networks are used to construct brain-wide structural connectivity by calculating gray matter volume correlations between brain regions.[16,17] However, such approaches face two major limitations. First, traditional structural covariance network approaches face inherent template-dependent limitations, as they require predefined anatomical atlases to parcellate brain regions before calculating inter-regional correlations. Different brain templates exhibit substantial variability in regional boundary definitions, particularly for complex structures like hippocampal subregions,[18] potentially introducing systematic bias that may mask genuine pathological network alterations characteristic of SCD. Second, individualized parsing constraints occur because structural covariance networks reflect population-level connectivity patterns and cannot capture the dynamic remodeling of individual gray matter networks,[19] which may be a key pathological feature during SCD conversion to MCI or AD.

The two-dimensional horizontal visibility graph (2DHVG) algorithm[20] provides an innovative solution to overcome the aforementioned limitations. Originally developed by Lacasa *et al.*[21] for time series analysis and subsequently extended to two-dimensional data, this method can operate directly on brain structural slices, constructing inter-pixel connectivity networks through pixel-level visibility criteria without relying on predefined brain region templates, thereby avoiding artificial biases introduced by segmentation errors. The horizontal visibility criterion states that two nodes are connected if and only if the line of sight between them remains unobstructed by any intermediate nodes with greater values. By preserving the original spatial distribution features of gray matter, 2DHVG can unbiasedly characterize pixel-level association patterns and reveal both global and local connectivity patterns between brain regions through graph-theoretic analysis,[20] offering more fine-grained and comprehensive characterization of brain features compared with traditional methods. This approach has demonstrated superior performance in image and signal classification tasks.[22–25]

This framework possesses several key mathematical properties that make it particularly suitable for neuroimaging analysis:[22] (i) it preserves local statistical characteristics of the original data through a parameter-free transformation, eliminating the need for arbitrary threshold selection; (ii) it effectively converts spatial distribution characteristics of gray matter structures into network topological representations amenable to rigorous graph-theoretical analysis; and (iii) it maintains both scale invariance and computational efficiency, enabling practical application to high-dimensional medical imaging data through slice-by-slice processing.

When applied to brain structural imaging, 2DHVG transforms pixel-level gray matter intensity distributions into connectivity networks, wherein clustering coefficients quantify local microstructural cohesion and betweenness centrality captures global information flow capacity.[26] This transformation is particularly relevant for investigating neurodegenerative diseases, as accumulating evidence suggests that pathological processes frequently manifest as disruptions in both local structural integrity and global network communication efficiency prior to the emergence of macroscopic atrophy detectable by conventional volumetric methods.[27] Thus, the 2DHVG approach offers a sensitive framework for detecting subtle network-level alterations that may serve as early biomarkers of cognitive decline, providing a template-free and individualized brain topological modeling tool at the pixel level.

Based on this, this paper introduces the 2DHVG analysis method to identify the differences in brain structural network features between SCD patients and healthy controls, providing novel insights into early SCD detection. Compared with traditional analysis methods, the 2DHVG method is not only computationally efficient but also visualizes the local connectivity and overall network characteristics of brain structures, which helps to reveal the underlying pathological network characteristics of SCD. Using this method, we aim to develop an accurate, convenient, and non-invasive early diagnostic tool that provides a novel analytical perspective and technical support for SCD identification.

2. Materials and methods

2.1. Data and subjects

Data used in this study were obtained from two publicly available datasets, including the Open Access Series of Imaging Studies 3 (OASIS-3)[28] and the Alzheimer's Disease Neuroimaging Initiative (ADNI), which have been described in Ref. [29]. Both datasets were collected according to the research ethics committees of each site, and informed consent was obtained from all participants. Inclusion criteria for both datasets encompassed: (i) subjects with intact cognitive functioning and appropriate diagnostic classifications; (ii) absence of neurodegenerative disorders, major psychiatric conditions, or other factors that could influence cognitive performance; (iii) availability of high-quality T1-weighted sMRI scans acquired within one year of clinical assessment; (iv) complete brain coverage meeting quality standards for analysis. In the OASIS-3 dataset, SCD was defined as self-reported memory decline relative to previous cognitive abilities, whereas individuals without such concerns were classified as normal aging (NA). In the ADNI dataset, SCD classification required subjective memory concerns confirmed by the Cognitive Change

Index questionnaire (total score ≥ 16 on the first 12 items), while those who did not meet this criterion were classified as NA. Following the inclusion criteria, the OASIS-3 dataset comprised 394 NA and 126 SCD subjects, while the ADNI dataset included 89 NA and 91 SCD participants. Please refer to Ref. [29] for detailed information regarding the specific inclusion criteria, subject classification procedures, and scanning parameters.

To systematically evaluate memory function and learning ability, several cognitive assessment scales closely related to early cognitive changes were selected from the ADNI database. These included the mini-mental state examination (MMSE), which serves as a global indicator of cognitive function, with higher scores reflecting better-preserved cognitive abilities. In addition, the ADNI_MEM composite memory score, derived from a series of memory-related tasks, provides a comprehensive assessment of memory performance. Previous ADNI studies have demonstrated its effectiveness in distinguishing between NA, SCD, and MCI groups, with higher scores indicating stronger memory function. Additionally, several components of the Rey auditory verbal learning test (RAVLT) were included: RAVLT.learning, which reflects verbal memory acquisition ability across successive learning phases and is widely used to assess hippocampal and related brain region functions; RAVLT.immediate, which measures short-term verbal memory capacity through immediate recall after the first presentation; and RAVLT.forgetting and RAVLT.perc.forgetting, which assess absolute and relative forgetting rates to evaluate information retention capacity. For all RAVLT measures, higher learning and immediate recall scores indicate better performance, while higher forgetting scores reflect greater memory decline and poorer retention ability. Table 1 summarizes the demographic information of the subjects involved in this study.

Table 1. The demographic information of the subjects involved in this study.

	OASIS-3			ADNI		
	NA	SCD	*P* value	NA	SCD	*P* value
Number of subjects	394	126	–	91	89	–
Years of age	68.89 ± 9.21	72.03 ± 8.88	$0.0004^{a,*}$	71.56 ± 5.12	73.13 ± 5.86	$0.0571^{a,c}$
Sex (male/female)	175/219	50/76	$0.3505^{b,c}$	35/56	38/51	$0.5629^{b,c}$
Years of education	16.01 ± 2.49	15.84 ± 2.69	$0.5211^{a,c}$	16.55 ± 2.39	16.83 ± 2.57	$0.4552^{a,c}$
MMSE	29.15 ± 1.16	29.00 ± 1.26	0.2260	28.96 ± 1.21	28.98 ± 1.26	0.9073
ADNI_MEM	–	–	–	1.10 ± 0.57	1.02 ± 0.59	0.3957
RAVLT.learning	–	–	–	6.14 ± 2.39	6.20 ± 2.42	0.8843
RAVLT.immediate	–	–	–	47.40 ± 10.76	45.52 ± 9.75	0.2245
RAVLT.forgetting	–	–	–	3.76 ± 3.15	3.68 ± 2.96	0.8616
RAVLT.perc.forgetting	–	–	–	34.30 ± 29.17	34.16 ± 28.07	0.9736

Abbreviations: NA, normal aging; SCD, subjective cognitive decline; MMSE, the Mini–Mental State Examination; positive and negative score values are presented as mean $\pm$ standard deviation. The symbol "–" indicates no calculation. [a]P-values were obtained using a two-sample two-tailed t-test. [b]P-values were obtained using a two-tailed chi-square test. [c]A P-value > 0.05 indicates that the difference between the two groups is not statistically significant. [*]A P-value < 0.05 indicates a statistically significant difference between the two groups.

2.2. Data pre-processing

Standard preprocessing using the DPARSFA toolbox[30] was conducted on all sMRI images, following the procedure outlined in Ref. [29]. In brief, after manual repositioning and skull stripping to remove non-brain tissues, spatial normalization to MNI space was performed using diffeomorphic anatomical registration through the exponentiated Lie algebra strategy.[31] Subsequently, tissue segmentation generated separate images for gray matter, white matter, and cerebrospinal fluid. Finally, intensity normalization was applied to scale the sMRI signals to a 0–255 grayscale range, thereby reducing inter-subject intensity variability and yielding high-quality gray matter images for further analysis.

2.3. Construction of 2DHVG

Following the completion of gray matter image preprocessing, we conducted axial slicing of the 3D brain gray matter images along the original scanning planes and subsequently constructed corresponding 2DHVGs for each slice. The core principle of this method involves treating each pixel in the image as a node in the network, where the grayscale value of each pixel corresponds to the height attribute of that node. Based on the 2DHVG visibility criterion, connectivity relationships are established between different pixel nodes, ultimately forming a comprehensive two-dimensional visibility graph network.

Formally, for a given 2D gray matter slice I with dimensions $H \times W$ (height $\times$ width), we construct an undirected graph $G = (V, E)$, where V represents the set of all pixel nodes and E denotes the edge set. Two nodes (i, j) and (i, c) located on the same row i are considered connected if and only if there is no intermediate pixel blocking their horizontal line of sight. Mathematically, this condition can be expressed as $\forall I \in [j+1, c-1], I(i,l) < \min(I(i,j), I(i,c))$, where $I(i,l)$ denotes the grayscale value at position (i,l).

The adjacency matrix A is defined as $A_{(i,j),(i,c)} = 1$ when the horizontal visibility condition is satisfied, and 0 otherwise. Please refer to Refs. [20,24] for more details of the 2DHVG method. Through this parameter-free transformation, the 2DHVG method effectively preserves the spatial distribution patterns of gray matter structures and converts these morphological features into network topological representations suitable for rigorous graph-theoretical analysis. The computational complexity of this algorithm is $O(HW^2)$, which remains tractable for typical MRI resolutions (e.g., 91×109 pixels per slice), rendering it well-suited for clinical applications. This approach offers a robust analytical framework for investigating gray matter structural differences while preserving both scale invariance and computational efficiency.

2.4. Implementation of feature extraction

Based on the constructed 2DHVGs, we extracted network metrics that capture complementary aspects of brain structural organization at both local and global levels. Specifically, node degree (ND), density (D), clustering coefficient (CC), and betweenness centrality (BC) were selected as key features.

2.4.1. Local connectivity metrics

For node i in the network, the node degree $ND_i = k_i$ represents the number of direct connections, quantifying local connectivity intensity. The network density is computed as $D = 2 \times E/[N \times (N-1)]$, where E is the total number of edges and N is the number of nodes, reflecting the overall compactness of network connectivity. The clustering coefficient is defined as $CC_i = 2 \times E_i/[k_i \times (k_i - 1)]$, where E_i denotes the number of actual edges between the neighbors of node i. Neurobiologically, high clustering indicates densely interconnected local structures, potentially reflecting preserved microstructural integrity.[32]

2.4.2. Global connectivity metrics

Betweenness centrality quantifies the importance of nodes in global information flow and is calculated as $BC_i = \sum_{s \neq i \neq t} \sigma_{st}(i)/\sigma_{st}$, where σ_{st} represents the total number of shortest paths from node s to node t, and $\sigma_{st}(i)$ denotes the number of those paths that traverse node i. Nodes with high BC values act as critical hubs facilitating inter-regional communication. Changes in BC may reflect disruptions in long-range connectivity, a hallmark of the AD continuum.[33]

2.4.3. Feature aggregation

For each subject, we extracted nodal ND, D, CC, and BC values from all nodes within each gray matter slice and then computed slice-wise averages to derive comprehensive network metrics that characterize individual-level structural topology. These metrics align with the dual syndrome hypothesis of neurodegeneration, wherein cognitive decline results from both local network fragmentation (reflected by ND, D, and CC) and global connectivity disruption (reflected by BC). This network-based characterization effectively captures abnormal alterations in connectivity patterns and topological organization in the brain structures of SCD patients,[34] providing a discriminative feature basis for subsequent classification tasks.

2.5. Feature dimensionality reduction

We employed principal component analysis (PCA) as the primary dimensionality reduction method, aiming to optimize the feature space while preserving essential discriminative information. Following a stratified random partitioning of the dataset into training and testing sets to maintain class balance, PCA was conducted on the training dataset to determine the optimal number of principal components. By analyzing the cumulative explained variance ratio, we dynamically identified the minimum number of principal components required to capture 95% of the total variance. This adaptive approach ensures that we retain only the essential components needed for optimal model performance while maintaining computational efficiency.

2.6. Machine learning framework and model optimization

We implemented a comprehensive machine learning framework that integrates the light gradient boosting machine (LightGBM) with stratified cross-validation (CV) to ensure robust model performance evaluation. Within the training dataset, we employed a 10-fold CV strategy combined with the synthetic minority over-sampling technique to effectively address class imbalance. During each CV iteration, the model was trained on nine folds and validated on the remaining fold, enabling us to evaluate performance across diverse data partitions. Throughout this process, we conducted hyperparameter optimization using the GridSearchCV strategy, systematically exploring key parameters such as learning rate, maximum depth, number of estimators, subsampling ratio, and class weighting strategies. The optimal hyperparameter configuration was selected based on the average ROC-AUC score across all CV folds, ensuring reliable and consistent model tuning. Finally, the best-performing model was applied to the independent test set to assess its generalization capability on unseen data.

3. Results

3.1. Visualization of the 2DHVG for SCD patients

Through constructing 2DHVGs for gray matter slices from all subjects, we can visualize the topological characteristics of brain structures. Figure 1 presents typical 2DHVG images from an SCD patient. These 2DHVG representations

of three different slices reveal connectivity patterns and variability of gray matter regions across different spatial levels, effectively reflecting the spatial heterogeneity of brain structures. Comparative analysis of these images demonstrates that 2DHVGs exhibit favorable sensitivity and expressive capability in characterizing brain regional topological structures and detecting subtle structural alterations.

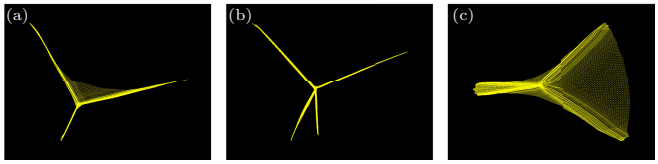


Fig. 1. Schematic diagram of 2DHVG construction across different gray matter slices: (a) z=30, (b) z=60, and (c) z=90.

3.2. Network feature extraction and dimensionality reduction

To quantify the topological characteristics of brain networks constructed based on 2DHVGs, we extracted network measures including node degree, network density, clustering coefficient, and betweenness centrality for each slice. Given that high-dimensional feature spaces may adversely affect classification performance, we performed PCA on the network feature vectors across all subjects.

First, all 700 subjects were randomly partitioned into training and testing sets at an 8:2 ratio. The training set was used for model training, whereas the testing set remained strictly independent. PCA was performed exclusively on the training set and subsequently applied to the testing set. As illustrated in Fig. 2(a), the first five principal components collectively explained over 70% of the total variance, while the first 60 principal components captured more than 95% of the variance, demonstrating that a substantial portion of the original information was preserved after dimensionality reduction.

To further evaluate the structure of the model's feature space and its classification performance, we examined the features extracted by PCA. As shown in Fig. 2(a), the first two principal components accounted for 46.4% and 8.8% of the total variance, respectively, resulting in a cumulative explained variance of 55.2%. To assess the model's ability to handle class imbalance, we generated the precision-recall (PR) curve to evaluate its performance in identifying the minority class (i.e., SCD) and quantified the overall discriminative ability using average precision (AP). As illustrated in Fig. 2(b), the model demonstrated robust performance in SCD detection, achieving an AP of 0.86. This result indicates that the model maintains excellent discriminative power and reliability even under imbalanced class distributions.

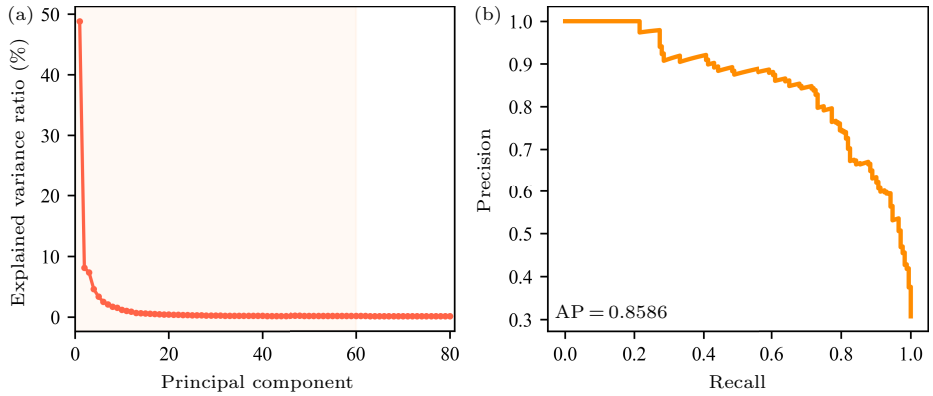


Fig. 2. (a) Explained variance ratio plot. The first 80 principal components are displayed to illustrate the variance distribution across the feature space. (b) Precision-recall curve of the model in the SCD vs. NA recognition task, with an average precision value of 0.86. AP denotes average precision.

3.3. SCD identification based on network features

Following feature extraction and dimensionality reduction, the derived network features were input into a LightGBM classifier to distinguish SCD patients from NAs. To ensure optimal model performance and robust generalization capability, a grid search combined with a 10-fold CV strategy was employed for systematic hyperparameter optimization. The main tuning parameters included: (i) learning rate set to 0.01–0.03 to control the weight update step size in each iteration; (ii) maximum depth limited to 4–6 to prevent overfitting in individual decision trees; (iii) number of weak classifiers set to 700–1000, representing the base learners in ensemble learning; (iv) subsample ratio set to 0.8 to enhance model generalization by controlling the sampling proportion in each training round; (v) class weight set to 'balanced' and 'None' to optimize loss function weight allocation under class imbalance conditions.

To account for the potential variability introduced by random data partitioning, we performed 100 independent runs and computed the average performance metrics to assess the model's generalization capability. The experimental results demonstrated that the proposed model achieved robust classification performance on the test set, with a mean AUC of 0.958, mean accuracy of 89.0%, mean sensitivity of 86.1%, mean specificity of 90.3%, and mean F1-score of 82.9%. The distribution of these performance metrics across all runs is il-

lustrated in Fig. 3(a). These results indicate that our method can effectively distinguish SCD patients from NA individuals, providing a reliable feature-based approach for early SCD identification.

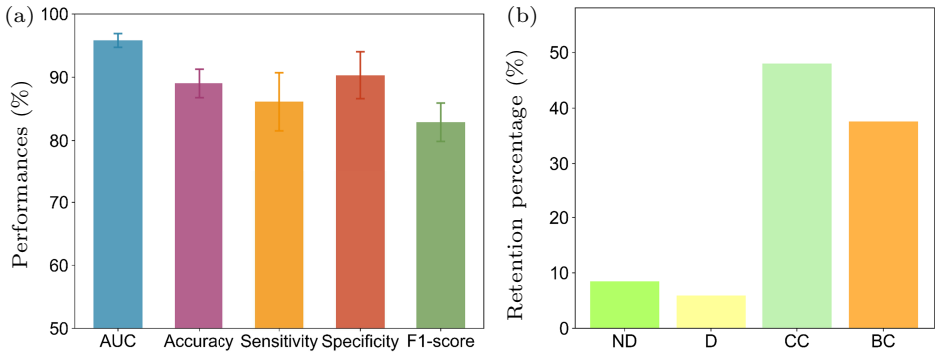


Fig. 3. (a) Error bar chart of classification performance metrics obtained from 100 independent runs on the test set. The model achieved an AUC of 0.958 ± 0.011, accuracy (ACC) of $89.0\% \pm 2.2\%$, sensitivity (SEN) of $86.1\% \pm 4.6\%$, specificity (SPE) of $90.3\% \pm 3.7\%$, and F1-score of $82.9\% \pm 3.0\%$. All results are presented as mean $\pm$ standard deviation. (b) Percentage distribution of retained frequencies for the four features, where ND, D, CC, and BC represent node degree, density, clustering coefficient, and betweenness centrality, respectively.

3.4. Comparison with existing methods

To validate the effectiveness of our proposed 2DHVG approach, we conducted systematic comparisons with both traditional morphological methods and popular classification algorithms.

3.4.1. Comparison with traditional morphological methods

We compared our method with three widely used morphological indicators: cortical thickness, gray matter volume, and gray matter density, all derived using the Desikan–Killiany atlas. After applying strict quality control measures during FreeSurfer processing, the final sample comprised 388 NAs and 125 SCDs from OASIS-3, and 87 NAs and 87 SCDs from ADNI. As shown in Table 2, our 2DHVG method significantly outperformed traditional morphological approaches across all metrics.

Table 2. Comparison of classification performances between traditional morphological methods and the introduced 2DHVG approach for SCD identification.

Metric	Thickness	Volume	Density	Our 2DHVG
AUC	0.646 ± 0.047	0.939 ± 0.011	0.941 ± 0.010	0.962 ± 0.007
Accuracy	0.507 ± 0.115	0.877 ± 0.023	0.876 ± 0.019	0.888 ± 0.024
Sensitivity	0.700 ± 0.196	0.817 ± 0.067	0.805 ± 0.081	0.885 ± 0.051
Specificity	0.422 ± 0.240	0.903 ± 0.041	0.908 ± 0.035	0.889 ± 0.046
F1-score	0.459 ± 0.051	0.801 ± 0.034	0.797 ± 0.037	0.828 ± 0.028

3.4.2. Comparison with popular classification methods

We conducted comprehensive comparisons with several widely used classification methods at two distinct levels. Initially, we evaluated three traditional machine learning classifiers, i.e., random forest, linear support vector machine (linear SVM), and the LightGBM model employed in our study, using identical network features derived from 2DHVGs to ensure a fair comparison. Additionally, we compared our approach with a convolutional neural network (CNN), which represents a fundamentally different paradigm. The CNN takes preprocessed sMRI images as direct input and automatically learns hierarchical feature representations through multiple convolutional and pooling layers, thus eliminating the need for manual feature extraction.

Table 3 demonstrates that among all compared methods, our employed LightGBM classifier achieved the highest performance, particularly excelling in overall discriminative ability (AUC: 0.958 ± 0.011) and sensitivity (0.861 ± 0.046). Notably, while the CNN approach showed competitive specificity, it exhibited considerable variability in sensitivity and F1-score, highlighting the stability and reliability advantages of our employed feature-based approach.

Table 3. Classification performances comparison among random forest, linear SVM, CNN, and our employed LightGBM methods for SCD identification.

Metric	Random forest	Linear SVM	CNN	Our LightGBM
AUC	0.926 ± 0.006	0.954 ± 0.012	0.911 ± 0.137	0.958 ± 0.011
Accuracy	0.848 ± 0.026	0.888 ± 0.017	0.868 ± 0.123	0.890 ± 0.022
Sensitivity	0.833 ± 0.058	0.843 ± 0.058	0.589 ± 0.416	0.861 ± 0.046
Specificity	0.854 ± 0.038	0.908 ± 0.018	0.991 ± 0.008	0.903 ± 0.037
F1-score	0.769 ± 0.037	0.821 ± 0.030	0.629 ± 0.437	0.829 ± 0.030

3.5. Discriminative characteristics

During the PCA dimensionality reduction process, components were selected based on a cumulative explained variance threshold of 95%. The four extracted network features were subjected to leave-one-out iterative selection, during which their occurrence frequencies were recorded to compute retention percentages. Figure 3(b) presents a bar chart illustrating the retention frequency percentages of the four features, reflecting their importance ranking in the classification task. Results demonstrated that clustering coefficient and betweenness centrality exhibited significantly higher retention frequencies than global efficiency and local efficiency, indicating their superior discriminative value in SCD identification.

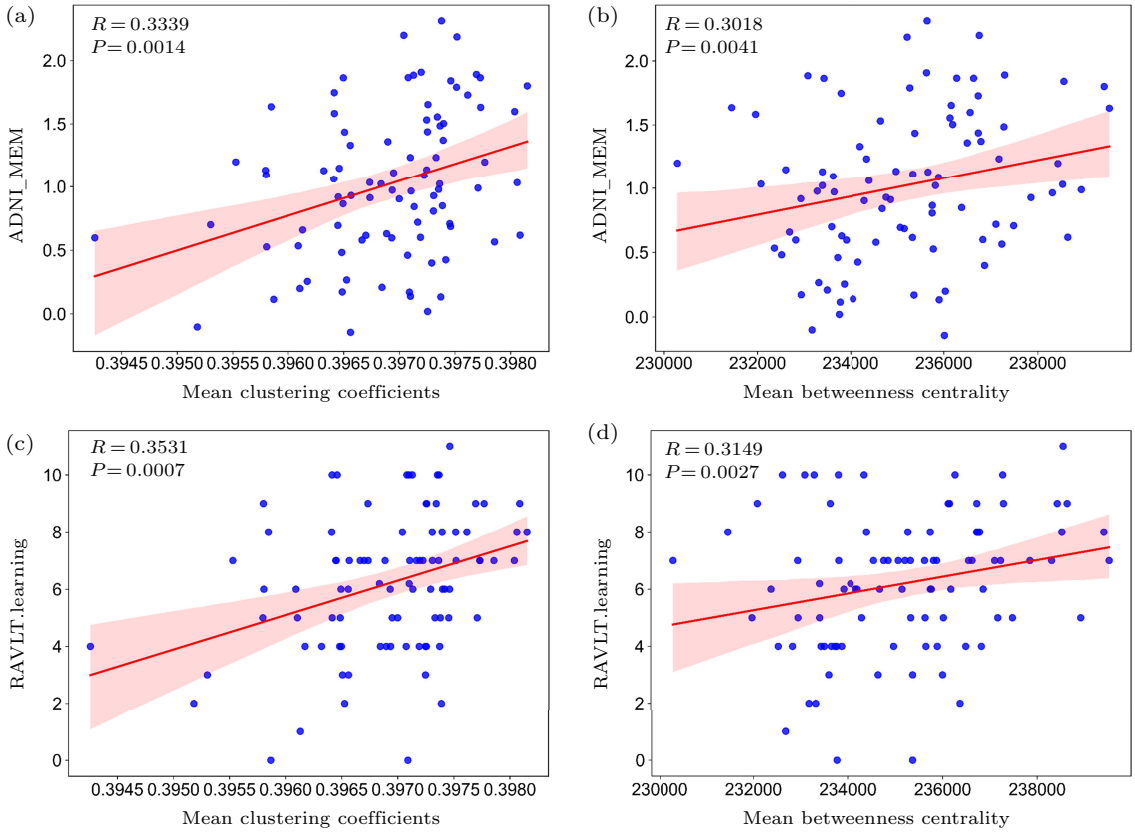


Fig. 4. Linear relationships between brain network metrics and cognitive scores. (a) Positive correlation between mean clustering coefficients and ADNI MEM scores with $R = 0.3339$ and $P = 0.0014$. (b) Positive correlation between mean betweenness centrality and ADNI MEM scores with $R = 0.3018$ and $P = 0.0041$. (c) Positive correlation between mean clustering coefficients and RAVLT.learning performance with $R = 0.3531$ and $P = 0.0007$. (d) Positive correlation between mean betweenness centrality and RAVLT.learning performance with $R = 0.3149$ and $P = 0.0027$.

Based on the feature importance analysis, we further investigated the correlations between clustering coefficient and betweenness centrality and cognitive assessment scales. Pearson correlation analysis revealed that both network features showed significant positive correlations with ADNI_MEM and RAVLT.learning scores in the SCD cohort.

As shown in Fig. 4, mean clustering coefficient demonstrated a moderate positive correlation with ADNI_MEM scores ($R = 0.3339$, $P = 0.0014$) and a stronger correlation with RAVLT.learning scores ($R = 0.3531$, $P = 0.0007$). Similarly, mean betweenness centrality showed significant positive correlations with both ADNI_MEM scores ($R = 0.3018$, $P = 0.0041$) and RAVLT.learning scores ($R = 0.3149$, $P = 0.0027$).

4. Discussion

In this study, we introduced a 2DHVG method for identifying patients with SCD. Based on sMRI data, this approach transforms gray matter structures into network connectivity relationships and extracts complex network features such as clustering coefficients and betweenness centrality. This method utilizes the advantages of 2DHVG in efficient graph construction and intuitive visualization, enabling clear representation of complex brain network topological properties. Our results demonstrate superior performance in SCD identification in terms of AUC, accuracy, sensitivity, specificity, and F1-score, confirming the method's potential for early SCD diagnosis. The dual cross-validation strategy employed during feature selection and model optimization further enhances model reliability and generalization capability, providing a promising technical pathway for neuroimaging-based SCD identification with significant clinical application value.

The comprehensive comparative analyses validate the superior performance of the 2DHVG approach, demonstrating substantial improvements over traditional morphological methods with an AUC of 0.958 ± 0.011. Among classification algorithms, our LightGBM-based approach achieved an optimal balance between sensitivity ($86.1\% \pm 4.6\%$) and specificity ($90.3\% \pm 3.7\%$), while deep learning methods like CNN showed considerable variability in sensitivity performance. These findings underscore the reliability of the 2DHVG method as a robust tool for SCD identification, offering consistent performance for medical applications.

Building upon these promising results, this study presents a novel application of the 2DHVG method for identifying patients with SCD, thereby extending the analytical scope beyond traditional brain network modeling. While prior research has primarily relied on structural covariance networks for brain network construction,[35,36] such approaches are in-

herently constrained by predefined anatomical parcellations. In contrast, the 2DHVG method constructs networks directly from pixel-level visibility relationships within individual brain slices, eliminating the need for atlas-based regional segmentation. This pixel-to-pixel connectivity mapping preserves the original spatial distribution of gray matter intensity patterns. It enables the detection of subtle microstructural variations that might otherwise be obscured by template-based averaging or boundary constraints. As a result, the method offers an unbiased representation of individual brain network topology, particularly valuable for detecting early pathological changes in SCD. Template-based parcellation may disrupt the intrinsic topological connections between brain regions, potentially overlooking subject-specific network alterations. Notably, while the 2DHVG method operates independently of templates, it retains the flexibility to integrate template-guided regional analysis when clinically warranted, offering adaptability not achievable with conventional covariance-based methods. By processing sMRI images slice by slice, the 2DHVG method achieves individualized brain topological modeling at the pixel level. It effectively preserves spatial microstructural information of gray matter regions and provides a more robust and flexible tool for early clinical identification of SCD, offering pixel-level network construction that directly captures individual structural variations without template bias.

Our findings are consistent with prior graph-theoretic investigations demonstrating structural alterations in brain networks of individuals with SCD.[37,38] Specifically, the observed abnormalities in CC suggest impaired local information processing within specialized neural circuits, even at the stage when individuals report only subjective cognitive complaints.[38] This finding aligns with evidence of increased modularity in SCD, potentially reflecting compensatory network reorganization in response to early dysfunction. Complementing these local alterations, reduced BC in key brain regions may indicate a diminished capacity of these critical hubs to integrate and relay information across distinct neural systems. Together, these network-level disruptions may contribute to a less efficient and less resilient global communication architecture, potentially underlying the subtle cognitive inefficiencies experienced by individuals with SCD.[37] Although recent studies have employed deep learning techniques for SCD identification, such models often suffer from limited interpretability due to their black-box nature.[39] In contrast, features derived from 2DHVG offer biologically meaningful insights: CC quantifies local structural cohesion, while BC measures hub vulnerability, both of which are well-established concepts in network neuroscience with demonstrated correlations to cognitive performance.

The significant correlations between the network metrics and cognitive performance provide convergent validity for the 2DHVG approach, aligning with the principle of structure-function coupling.[40] The positive correlation between mean CC and both ADNI_MEM scores ($R = 0.3339$, $P = 0.0014$) and RAVLT learning scores ($R = 0.3531$, $P = 0.0007$) suggests that brain regions with tighter local connections exhibit better memory retention and learning capacity. Lower CC values indicate local connectivity disruption correlating with faster clinical progression in AD,[41] while higher clustering levels suggest stronger local integration, providing stable micro-network foundations for information processing and memory trace formation.[42,43] Moreover, the positive correlation between mean BC and ADNI_MEM ($R = 0.3018$, $P = 0.0041$) as well as RAVLT learning scores ($R = 0.3149$, $P = 0.0027$) indicates that key hub nodes serving as network bridges play central roles in maintaining memory function and facilitating cross-regional information propagation between functional modules.[44,45] Combining CC and BC captures both local connectivity integrity and global communication hub characteristics, providing a comprehensive framework for characterizing early AD topological reorganization.[42,46]

The relationship between topological features and cognitive performance observed in this study aligns with findings from previous resting-state functional connectivity and gray matter atlas studies,[43,47] suggesting that early structural network degeneration in AD may lead to declined learning performance by weakening the synergy between local clusters and global hubs. Given the sensitivity of ADNI_MEM to working memory, declarative memory, and verbal recall,[48] and the RAVLT task's ability to reflect the complete process of new information encoding, storage, and retrieval,[49] these metrics provide clinically meaningful interpretations for understanding memory-learning impairments from a brain network mechanism perspective. In contrast, when applying the same analysis to NA data, network metrics showed weak correlations with cognitive scores, with correlation coefficients generally below 0.3.

The 2DHVG method processes axial slices in a layer-by-layer manner, effectively preserving spatial continuity along the z-axis. While each slice is modeled with an independently constructed network, the integration of topological features across multiple layers enables the capture of comprehensive three-dimensional brain structural characteristics. This slice-wise strategy aligns with the conventional layer-by-layer analysis widely used in traditional neuroimaging,[50] ensuring computational efficiency and facilitating practical application to high-dimensional medical imaging data.

The core advantage of our 2D approach lies in its ability to construct networks at the pixel level. By establishing inter-pixel connectivity through the horizontal visibility criterion, this method operates directly on brain structural slices without relying on predefined brain region templates, thus avoiding ar-

tificial biases caused by template segmentation errors. This pixel-to-pixel connectivity mapping preserves the original spatial distribution patterns of gray matter intensity, enabling the detection of subtle structural variations that might be obscured by template-based approaches. This capability is particularly critical in SCD, where early pathological changes have not yet progressed to macroscopic atrophy detectable by conventional volumetric methods.

From a neuroinformatics perspective, the 2DHVG approach enables individualized brain topological modeling by preserving spatial adjacency and tissue continuity information inherent in the original sMRI data. Its parameter-free transformation retains the local statistical properties of the raw data while efficiently translating the spatial distribution patterns of gray matter structures into network-based topological representations suitable for rigorous graph-theoretical analysis. Our findings demonstrate that two-dimensional topological representations not only effectively capture the underlying neuropathological patterns but also preserve high interpretability.

Despite the satisfactory performance of the 2DHVG method in SCD patient identification, several limitations should be considered. First, this approach constructs networks using 2D slices from gray matter images, whereas the brain is inherently a 3D structure. By processing each axial slice independently, our method does not explicitly capture inter-slice connectivity information along the z-axis, which may omit some vertical relationships between brain regions. However, the employed slice sequence approach partially mitigates this limitation by effectively preserving spatial continuity along the z-axis through multi-layer feature integration. Direct construction of 3D visibility graphs would impose excessive computational demands for typical brain sMRI data, making the adopted 2D strategy a computationally efficient alternative that still achieves a mean AUC exceeding 0.95. Future research may explore hybrid models that dynamically couple multi-layer slices to improve spatial completeness and explicitly incorporate inter-slice relationships. Second, the sample size was limited by data availability and practical challenges in recruiting SCD patients. Although the current study achieved good classification performance, larger-scale validation studies are necessary to confirm the generalizability of the results.

5. Conclusion

This study introduces a novel sMRI network construction method based on 2D visibility graphs and applies it to the early identification of SCD patients. The results demonstrate that the topological features of this network model exhibit excellent identification performance, achieving a mean AUC of over 0.95, which fully validates its application value in early SCD identification. Through 2D slice network feature analysis, this method clearly reveals characteristic differences in brain structural networks of SCD patients, providing a new quantitative tool for early SCD identification and classification. The visibility graph-based brain network model shows broad application prospects in the field of neurodegenerative disease identification and research.

Acknowledgments

We acknowledge the OASIS-3 Principal Investigators (T. Benzinger, D. Marcus, and J. Morris) and OASIS-3 grants (NIH P30AG066444, P50AG00561, P30NS09857781, P01AG026276, P01AG003991, R01AG043434, UL1TR000448, and R01EB009352). AV-45 doses were provided by Avid Radiopharmaceuticals, a wholly owned subsidiary of Eli Lilly. We also gratefully acknowledge the contributions from the ADNI project. The ADNI was launched in 2003 as ADNI-1, with subsequent phases including ADNI-GO (2009), ADNI-2 (2010), and ADNI-3 (2016). The ADNI study has observed individuals diagnosed as cognitively normal or with varying degrees of cognitive impairment since 2005. Project updates and more detailed study information can be found at http://www.adni-info.org.

Project supported by the National Key R&D Program of China (Grant No. 2023YFF1204803), the Natural Science Foundation of Jiangsu Province (Grant No. BK20190736), and the Natural Science Foundation of China (Grant No. 81701346).

References

[1] Jessen F, Amariglio R E, *et al.* 2014 *Alzheimers Dement.* **10** 844
[2] Jack C R, Bennett D A, Blennow K, Carrillo M C, Dunn B, Haeberlein S B, Holtzman D M, Jagust W, Jessen F, Karlawish J, Liu E, Molinuevo J L, Montine T, Phelps C, Rankin K P, Rowe C C, Scheltens P, Siemers E, Snyder H M, Sperling R, Elliott C, Masliah E, Ryan L and Silverberg N 2018 *Alzheimers Dement.* **14** 535
[3] Vemuri P and Jack C R 2010 *Alzheimers Res. Ther.* **2** 23
[4] Peter J, Scheef L, Abdulkadir A, Boecker H, Heneka M, Wagner M, Koppara A, Klöppel S, Jessen F and Alzheimer's Disease Neuroimaging Initiative 2014 *Alzheimers Dement.* **10** 99
[5] Arrondo P, Elía-Zudaire Ó, Martí-Andrés G, Fernández-Seara M A and Riverol M 2022 *Alzheimers Res. Ther.* **14** 98
[6] Striepens N, Scheef L, Wind A, Popp J, Spottke A, Cooper-Mahkorn D, Suliman H, Wagner M, Schild H H and Jessen F 2010 *Dement. Geriatr. Cogn. Disord.* **29** 75
[7] Doherty B M, Schultz S A, Oh J M, Koscik R L, Dowling N M, Gallagher C L, Carlsson C M, Bendlin B B, LaRue A, Hermann B P, Rowley H A, Asthana S, Sager M A, Johnson S C and Okonkwo O C 2015 *Alzheimers Dement.* **1** 160
[8] Kim M J, Seo S W, Kim G H, Kim S T, Lee J M, Qiu A and Na D L 2013 *Arch. Gerontol. Geriatr.* **57** 110
[9] Perrotin A, De Flores R, Lamberton F, Poisnel G, La Joie R, De La Sayette V, Mézenge F, Tomadesso C, Landeau B, Desgranges B and Chételat G 2015 *J. Alzheimers Dis.* **48** S141
[10] Liang L, Zhao L, Wei Y, Mai W, Duan G, Su J, Nong X, Yu B, Li C, Mo X, Wilson G, Deng D and Kong J 2020 *Front. Aging Neurosci.* **12** 64
[11] Jessen F, Feyen L, Freymann K, Tepest R, Maier W, Heun R, Schild H H and Scheef L 2006 *Neurobiol. Aging* **27** 1751
[12] Ryu S Y, Lim E Y, Na S, Shim Y S, Cho J H, Yoon B, Hong Y J and Yang D W 2017 *Int. Psychogeriatr.* **29** 785

[13] Li W, Yue L and Xiao S 2022 *Front. Psychiatry* **13** 950270

[14] Song J, Yang H, Yan H, Lu Q, Guo L, Zheng H, Zhang T, Lin B, Zhao Z, He C and Shen Y 2024 *Brain Imaging Behav.* **18** 1536

[15] Zhang M and Huang P 2021 *Int. J. Med. Radiol.* **44** 373

[16] Han S, Zheng R, Li S, Liu L, Wang C, Jiang Y, Wen M, Zhou B, Wei Y, Pang J, Li H, Zhang Y, Chen Y and Cheng J 2023 *Psychol. Med.* **53** 2146

[17] Liu J, Tao W, Guo X, Kwapong W R, Ye C, Wang A, Wu X, Wang Z and Liu M 2023 *Investig. Ophthalmol. Vis. Sci.* **64** 40

[18] De Flores R, Berron D, Ding S, Ittyerah R, Pluta J B, Xie L, Adler D H, Robinson J L, Schuck T, Trojanowski J Q, Grossman M, Liu W, Pickup S, Das S R, Wolk D A, Yushkevich P A and Wisse L E M 2020 *Hippocampus* **30** 545

[19] Vermunt L, Dicks E, Wang G, *et al.* 2020 *Brain Commun.* **2** fcaa102

[20] Iacovacci J and Lacasa L 2018 *IEEE Trans. Pattern Anal. Mach. Intell.* **42** 974

[21] Lacasa L, Luque J, Luque B, Ballesteros F and Nuño J C 2008 *Proc. Natl. Acad. Sci. USA* **105** 4972

[22] Wen T, Chen H and Cheong K H 2022 *Nonlinear Dyn.* **110** 2979

[23] Pei L, Li Z and Liu J 2021 *Chaos* **31** 013128

[24] Ni H J, Du R Y, Liang L, Hua L L, Zhu L H and Qin J L 2023 *Chin. Phys. B* **32** 078501

[25] Ma L, Ren Y L, He A J, Cheng D Q and Yang X D 2023 *Chin. Phys. B* **32** 110506

[26] Derbie A Y, Altaye M, Wang J, Allahverdy A, He L, Tamm L and Parikh N A 2025 *Commun. Biol.* **8** 345

[27] Sharma R and Joshi S D 2025 *Ann. Neurosci.* **32** 21

[28] LaMontagne P J, Benzinger T L, Morris J C, Keefe S, Hornbeck R, Xiong C, Grant E, Hassenstab J, Moulder K, Vlassenko A G, Raichle M E, Cruchaga C and Marcus D 2019 *Ann. Neurosci.* **32** 21

[29] Ni H, Xue J, Qin J and Zhang Y 2024 *Comput. Methods Programs Biomed.* **254** 108281

[30] Yan C G and Zang Y F 2010 *Front. Syst. Neurosci.* **4** 13

[31] Ashburner J 2007 *NeuroImage* **38** 95

[32] Hocking M C, Schultz R T, Yerys B E, Minturn J E, Fantozzi P and Herrington J D 2024 *J. Neurooncol.* **169** 247

[33] Dupré N, Drieu A and Joutel A 2024 *J. Clin. Invest.* **134** e172841

[34] Shu N, Wang X, Bi Q, Zhao T and Han Y 2018 *Radiology* **286** 229

[35] Wang J, Wang X, Xia M, Liao X, Evans A and He Y 2015 *Front. Hum. Neurosci.* **9** 386

[36] He Y, Chen Z J and Evans A C 2007 *Cereb. Cortex* **17** 2407

[37] Deng S, Tan S, Song X, Lin X, Yang K and Li X 2024 *CNS Neurosci. Ther.* **30** e14859

[38] Xu X, Chen P, Xiang Y, Xie Z, Yu Q, Zhou X and Wang P 2022 *Front. Aging Neurosci.* **14** 965923

[39] Dhavamani L, Joshi S V, Kothapalli P K V, Elangovan M, Putchanuthala R B and Senthamil Selvan R 2025 *Microsc. Res. Tech.* **88** 1115

[40] Jin J, Ma J, Wu J J, Lu J J, Lu H Y, Zheng M X, Hua X Y and Xu J G 2025 *CNS Neurosci. Ther.* **31** e70205

[41] Verfaillie S C J, Slot R E R, Dicks E, Prins N D, Overbeek J M, Teunissen C E, Scheltens P, Barkhof F, van der Flier W M and Tijms B M 2018 *Hum. Brain Mapp.* **39** 3143

[42] He Y, Chen Z and Evans A 2008 *J. Neurosci.* **28** 4756

[43] Tijms B M, Möller C, Vrenken H, Wink A M, De Haan W, Van Der Flier W M, Stam C J, Scheltens P and Barkhof F 2013 *PLoS ONE* **8** e58921

[44] Rubinov M and Sporns O 2010 *NeuroImage* **52** 1059

[45] Van Den Heuvel M P and Sporns O 2013 *Trends Cogn. Sci.* **17** 683

[46] Dai Z and He Y 2014 *Neurosci. Bull.* **30** 217

[47] Wang J, Zuo X, Dai Z, Xia M, Zhao Z, Zhao X, Jia J, Han Y and He Y 2013 *Biol. Psychiatry* **73** 472

[48] Crane P K, Carle A, Gibbons L E, Insel P, Mackin R S, Gross A, Jones R N, Mukherjee S, Curtis S M, Harvey D, Weiner M and Mungas D 2012 *Brain Imaging Behav.* **6** 502

[49] Estévez-González A, Kulisevsky J, Boltes A, Otermín P and García-Sánchez C 2003 *Int. J. Geriatr. Psychiatry* **18** 1021

[50] Li X, Zhou Y, Dvornek N, Zhang M, Gao S, Zhuang J, Scheinost D, Staib L H, Ventola P and Duncan J S 2021 *Med. Image Anal.* **74** 102233